OPEN ACCESS Freely available online

PLoS one

Effect of $Ca_v\beta$ Subunits on Structural Organization of $Ca_v1.2$ Calcium Channels

Evgeny Kobrinsky[•], Parwiz Abrahimi[•], Son Q. Duong, Sam Thomas, Jo Beth Harry, Chirag Patel, Qi Zong Lao, Nikolai M. Soldatov*

National Institute on Aging, National Institutes of Health, Baltimore, Maryland, United States of America

Abstract

Background: Voltage-gated $Ca_v1.2$ calcium channels play a crucial role in Ca^{2+} signaling. The pore-forming α_{1C} subunit is regulated by accessory $Ca_v\beta$ subunits, cytoplasmic proteins of various size encoded by four different genes ($Ca_v\beta_1$ - β_4) and expressed in a tissue-specific manner.

Methods and Results: Here we investigated the effect of three major $Ca_v\beta$ types, β_{1b}, β_{2d} and β_3, on the structure of $Ca_v1.2$ in the plasma membrane of live cells. Total internal reflection fluorescence microscopy showed that the tendency of $Ca_v1.2$ to form clusters depends on the type of the $Ca_v\beta$ subunit present. The highest density of $Ca_v1.2$ clusters in the plasma membrane and the smallest cluster size were observed with neuronal/cardiac β_{1b} present. $Ca_v1.2$ channels containing β_3, the predominant $Ca_v\beta$ subunit of vascular smooth muscle cells, were organized in a significantly smaller number of larger clusters. The inter- and intramolecular distances between α_{1C} and $Ca_v\beta$ in the plasma membrane of live cells were measured by three-color FRET microscopy. The results confirm that the proximity of $Ca_v1.2$ channels in the plasma membrane depends on the $Ca_v\beta$ type. The presence of different $Ca_v\beta$ subunits does not result in significant differences in the intramolecular distance between the termini of α_{1C}, but significantly affects the distance between the termini of neighbor α_{1C} subunits, which varies from 67 Å with β_{1b} to 79 Å with β_3.

Conclusions: Thus, our results show that the structural organization of $Ca_v1.2$ channels in the plasma membrane depends on the type of $Ca_v\beta$ subunits present.

Citation: Kobrinsky E, Abrahimi P, Duong SQ, Thomas S, Harry JB, et al. (2009) Effect of $Ca_v\beta$ Subunits on Structural Organization of $Ca_v1.2$ Calcium Channels. PLoS ONE 4(5): e5587. doi:10.1371/journal.pone.0005587

Editor: Arnold Schwartz, University of Cincinnati, United States of America

Received March 17, 2009; **Accepted** April 18, 2009; **Published** May 18, 2009

Funding: This work was supported by the NIA Intramural Research Program (Z01 AG000294-08 to NMS). The funders had no role in study design, data collection and analysis, decision to publish, or preparation of the manuscript.

Competing Interests: The authors have declared that no competing interests exist.

* E-mail: soldatovN@grc.nia.nih.gov

• These authors contributed equally to this work.

Introduction

Voltage-gated $Ca_v1.2$ calcium channels react to membrane depolarization by creating a rapid and transient increase in intracellular free Ca^{2+} concentration, thereby playing an essential role in initiation of calcium signaling in a wide variety of cells [1]. In order to exhibit this function, $Ca_v1.2$ calcium channels require association of the pore-forming α_{1C} subunit with accessory $Ca_v\beta$ and $\alpha_2\delta$ subunits as well as calmodulin. Calcium channels are clustered rather than evenly distributed along the surface membrane of neurons [2–4] and cardiac myocytes [5–7]. Single-molecule imaging of the functional recombinant $EYFP_N$-$\alpha_{1C}/\beta_{2a}/\alpha_2\delta$ channels revealed clusters composed of ~40 channels [8]. In neuronal cell bodies and proximal dendrites in hippocampus and cerebral cortex, $Ca_v1.2$ clusters of 1.5–2 μm in diameter were observed with anti-α_{1C} antibody [9]. Using electron microscopy in bird and amphibian cardiac muscle [5,6] and immuno-gold labeling in mammalian ventricular myocytes [7,10] it was shown that $Ca_v1.2$ clusters are loosely tethered to ryanodine receptors (RyR) of the sarcoplasmic reticulum. Although association of calcium channels and ryanodine receptors appears to be weaker in cardiac myocytes than in skeletal muscle [11] and may involve different mechanisms of coupling [12], $Ca_v1.2$ clustering is essential for excitation-contraction coupling [13,14].

Little is known about the factors affecting the structure of $Ca_v1.2$ clusters or the mechanisms of their formation. Because the carboxyl-terminal "IQ" region of α_{1C} mediates the calmodulin-dependent Ca^{2+}-induced inactivation of the channel [15–18], it is reasonable to suggest that both calmodulin and the cytoplasmic 750-amino acid C-tail of α_{1C} have a role in the formation and maintenance of the $Ca_v1.2$ clusters. Indeed, a splice variant of α_{1C} ($\alpha_{1C,86}$) deprived of IQ does not show a distinct tendency to form clusters [19]. The role of IQ sequences in intermolecular interactions between neighboring α_{1C} molecules was experimentally confirmed in recent diffraction study [20]. The impact of bulky cytoplasmic $Ca_v\beta$ subunits on $Ca_v1.2$ structure and clustering is not known. $Ca_v\beta$ subunits are important differential modulators of the electrophysiological properties of calcium channels [21–23]. These peripheral proteins of variable size are encoded by four different genes ($Ca_v\beta_1$ - β_4), some of them being subject to alternative splicing [24]. They have a common binding site in the cytoplasmic linker between repeats I and II of α_{1C}

known as the α-interaction domain (AID) [25]. Here, we applied total internal fluorescence reflection (TIRF) and three-color FRET microscopy to assess the effects of $Ca_v\beta$ on cluster size and density of $Ca_v1.2$ as well as to measure inter- and intramolecular distances between the N- and C-termini of α_{1C} and the N-tails of β_{1b}, β_{2d} and β_3. Our results demonstrated that $Ca_v1.2$ channels form plasma membrane clusters and revealed the effect of the type of $Ca_v\beta$ present on molecular distances and packing of the channels.

Results

Differential effect of $Ca_v\beta$ subunits on cluster organization of $Ca_v1.2$ channels

$Ca_v1.2$ calcium channels retain functional activity after fusion of fluorescent proteins to the N- and C-termini of α_{1C} and to the N-terminus of $Ca_v\beta$. In our experiments, we labeled α_{1C} at the N-tail with monomeric mVenus ($V\alpha_{1C}$) and/or at the C-tail with monomeric mCerulean ($\alpha_{1C}C$) [26]. To investigate the effect of $Ca_v\beta$ subtype on size and density of $Ca_v1.2$ clusters, we chose three major $Ca_v\beta$ variants, neuronal/cardiac β_{1b} [27], cardiac β_{2d} [28,29] and neuronal/cardiac/vascular β_3 [30–32], which is the predominant $Ca_v\beta$ subunit in vascular smooth muscle cells [31,33]. The more commonly used β_{2a} was excluded from the experiments because its N-tail is palmytoylated and anchored to the inner leaflet of the plasma membrane.

Fluorescent microscopy is a convenient approach to detect clusters of recombinant calcium channels as fluorescent foci or groupings of labeled molecules [34]. In this study, we used TIRF microscopy to visualize $Ca_v1.2$ clusters on the basal plasma membrane. Wavelet transform was used for the detection of clusters (see Methods and Figure 1*A*) to estimate the effect of the type of $Ca_v\beta$ present on the $Ca_v1.2$ clusters size (Figure 1*B*) and density (defined here as number of clusters per μm^2 of the plasma membrane, Figure 1*C*). The smallest $Ca_v1.2$ clusters were observed with β_{1b} present. $Ca_v1.2$ clusters were significantly ($P<0.001$) larger with β_{2d} (by ~20%) and β_3 present (by ~30%) (Figure 1*B*). We also found that the average density of the $V\alpha_{1C}/\beta_{1b}$ clusters in the plasma membrane was 2.5 times higher ($P<0.01$) than $V\alpha_{1C}/\beta_3$, with β_{2d} again taking an intermediate value (Figure 1*C*). Thus, $Ca_v\beta$ subunits differentially regulate the architecture of the $Ca_v1.2$ clusters.

In principle, the close proximity of channels within a cluster may generate intermolecular FRET between the V and C fluorophores of neighboring $V\alpha_{1C}C$ channels. This intermolecular FRET should be absent outside of clusters, where only intramolecular FRET should occur. The $V\alpha_{1C}C/\alpha_2\delta/\beta_3$ channel was expressed in COS1 cells and two-color TIRF-FRET was measured inside and outside of clusters identified by wavelet transform. Based on FRET efficiency, a V-C distance (*r*)-frequency histogram of the total number of pixels within clusters revealed a possible bi-modal distribution, where a second (intermolecular) component of FRET is seen within clusters (Figure 2*A*) but not outside of the clusters (Figure 2*B*). Because TIRF microscopy captures only a small fraction of the cell plasma membrane, we used epifluorescent three-color FRET microscopy to quantitatively analyze the effect of $Ca_v\beta$ subtype on inter- and intra-molecular distance of $Ca_v1.2$ channels.

The type of $Ca_v\beta$ present does not affect intramolecular distance between the N- and C-termini of the α_{1C} subunit

We investigated the effect of $Ca_v\beta$ subtype on molecular distances in $Ca_v1.2$ channels by three-color FRET between $V\alpha_{1C}C$ and tagRFP (Rβ) fused to N-termini of β_{1b}, β_{2d} and β_3. The advantage of three-color FRET cell microscopy applied to multisubunit complexes is that the method simultaneously detects the relative arrangement of the three different fluorophores (C, V and R) at a distance $\leq 2\times R_o$, where R_o is the Förster radius ($R_{o(C\text{-}V)} = 53$ Å; $R_{o(V\text{-}R)} = 58$ Å; $R_{o(C\text{-}R)} = 51$ Å). Both mCerulean and mVenus are close analogs of GFP and can be approximated by a cylinder of 32×48 Å [35]. However, tagRFP [36], a monomeric analog of eqFP611, is larger in size and can be approximated by a cylinder of 34×54 Å [37]. Use of monomeric forms of fluorescent proteins excludes artifacts due to dimerization after expression [38]. The labeled constructs were co-expressed with $\alpha_2\delta$ in two different combinations as shown in Figure 3, and three-color FRET was measured using a multicube system [39]. Although membrane potential was not controlled during experiments, it was found to be on average -10.0 ± 3.3 mV (n = 5) indicating that channels were predominantly in an inactivated state. In each fluorescent cell image, region of interest (ROI) was determined using a standard procedure as described earlier [40]. Within this ROI, only pixels with donor/acceptor ratio from 0.2 to 5 (Figure 4, left panels) were selected for further analysis [41]. FRET efficiency was determined according to [42] (Figure 4, middle panels) and

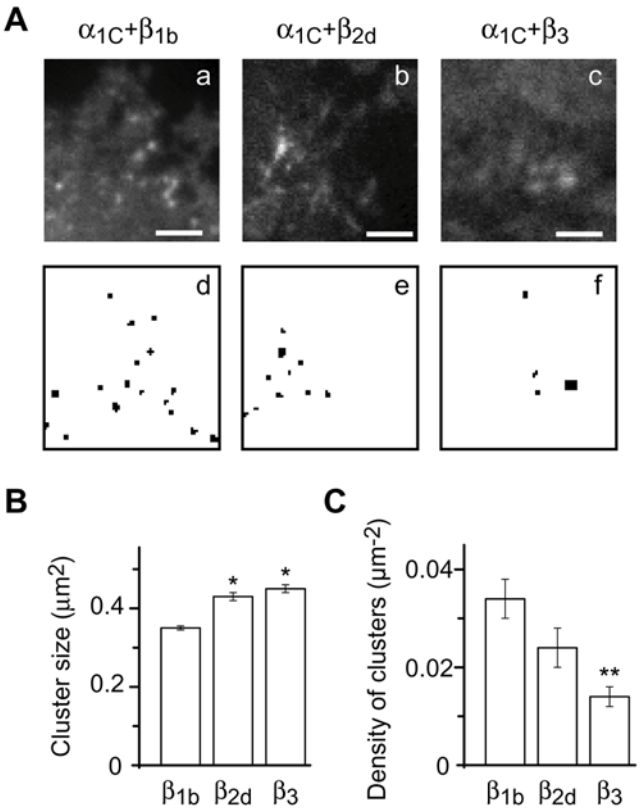

Figure 1. Effect of $Ca_v\beta$ subunits on cluster organization of $Ca_v1.2$ channels. (*A*) TIRF images (*a–c*) and wavelet-derived clusters (*d–f*) of $Ca_v1.2$ channels containing β_{1b} (*a,d*), β_{2d} (*b,e*) or β_3 (*c,f*). Scale, 4.5 μm. (*B*) Dependence of the average size of $Ca_v1.2$ clusters on the type of $Ca_v\beta$ present. β_{1b}, mean size±SEM, 0.360±0.005 μm^2 (number of clusters analyzed m = 1253); β_{2d}, 0.430±0.013 mm^2 (m = 270); β_3, 0.450±0.017 μm^2 (m = 205). *, $P<0.001$ relative to β_{1b}. (*C*) Dependence of the number of $Ca_v1.2$ clusters (normalized to the area measured and defined as density) on the type of $Ca_v\beta$ present. β_{1b}, mean number±SEM, 0.034±0.004 mm^{-2} (number of cells n = 27); β_{2d}, 0.024±0.04 μm^{-2} (n = 30); β_3, 0.014±0.02 μm^{-2} (n = 22). **, $P<0.01$ relative to β_{1b}. $V\alpha_{1C}$ was co-expressed with $\alpha_2\delta$ and indicated $Ca_v\beta$ in COS1 cells.
doi:10.1371/journal.pone.0005587.g001

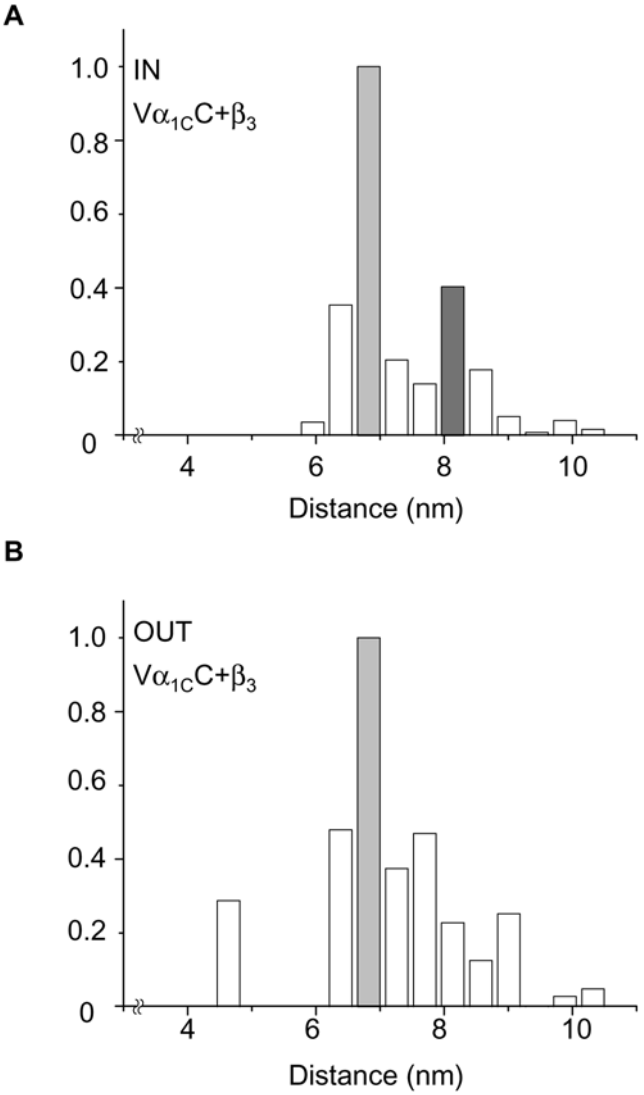

Figure 2. Intramolecular vs. intermolecular FRET in $V\alpha_{1C}C$ revealed in TIRF images. $V\alpha_{1C}C$, $\alpha_2\delta$ and β_3 were co-expressed in COS1 cells. Two-color FRET was measured in TIRF images and converted into distances *r* between V and C as described in Methods. Shown are normalized cumulative histograms (n = 11) for *r* calculated for ROI inside clusters (*A*, total number of pixels m = 231) and outside clusters (*B*, m = 3908) identified by wavelet transform. The same intramolecular ($r_{V\text{-}C}$) distance ≈6.8 nm (light gray bars) was observed both inside and outside clusters, while intermolecular ($r_{V\sim C}$) distance ≈8.1 nm was observed only in clusters (dark gray).
doi:10.1371/journal.pone.0005587.g002

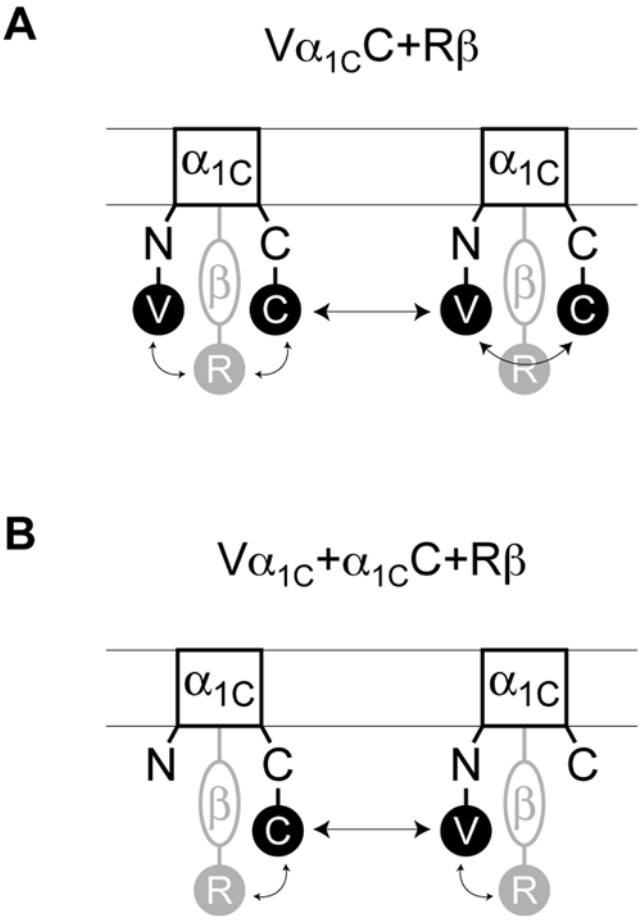

Figure 3. Investigated combinations of the labeled α_{1C} and β subunits for three color FRET measurements. $V\alpha_{1C}C$ and Rβ (A) and $V\alpha_{1C}$, $\alpha_{1C}C$ and Rβ (B) were co-expressed with $\alpha_2\delta$ (not shown). Arrows indicate revealed intramolecular and intermolecular distances.
doi:10.1371/journal.pone.0005587.g003

then converted to the distance (*r*) between donor and acceptor (right panel) according to [43].

Results of our measurements revealed that the tested $Ca_v\beta$ subunits did not affect intramolecular distance between the N- and C-termini of α_{1C}. Measurement of FRET in the double-labeled $V\alpha_{1C}C$ co-expressed with $\alpha_2\delta$ and $R\beta_{1b}$, $R\beta_{2d}$ or $R\beta_3$ showed that the intramolecular distance $r_{C\text{-}V}$ between V and C did not vary significantly and was on average 68–69 Å, independent of the type of co-expressed $Ca_v\beta$ (Figure 4, *A–C*; see Table 1 for statistics).

Estimation of $r_{C\text{-}V}$ in the absence of $Ca_v\beta$ was not possible because of poor plasma membrane targeting by $V\alpha_{1C}C/\alpha_2\delta$ under such conditions. To overcome this problem, we co-expressed $V\alpha_{1C}C$ and $\alpha_2\delta$ with tagRFP-labeled β_2CED, a 42-amino acid fragment of β_2 subunits which does not bind to AID, but interacts with the IQ region of the α_{1C} subunit C-terminus, facilitates voltage gating and stimulates surface expression of the channel [44]. Results of FRET measurements showed $r_{C\text{-}V} = 68 \pm 1$ Å (n = 22), essentially the same distance as that estimated when AID was occupied by $Ca_v\beta$. Taken together, these results of our study suggest that type of $Ca_v\beta$ subunits present does not significantly affect the intramolecular distance between the N- and C-termini of α_{1C} in $Ca_v1.2$ calcium channels.

Intermolecular distance between the α_{1C} subunit N- and C-termini depends on the type of $Ca_v\beta$ present

Fitting of FRET data obtained with β_{2d} and β_3 to a sum of two Gaussian distributions (Table 1) revealed a statistically significant second component of $V\alpha_{1C}C$ FRET (Figure 5). Arising from neighboring $V\alpha_{1C}C$ molecules, this FRET provided estimates for the intermolecular distances ($r_{C\sim V}$) that were significantly different for β_{2d} (72±3 Å, n = 5) and β_3 (77±3 Å, n = 6). To verify our intermolecular distance measurements, we co-expressed a mixture of $V\alpha_{1C}$ and $\alpha_{1C}C$ along with $R\beta_{1b}$, $R\beta_{2d}$ or $R\beta_3$ (Figure 4, *D–F*). Any FRET between V and C in this recombinant system must be intermolecular FRET between termini of neighboring channels. Results, presented in Table 1, showed that intermolecular distances $r_{C\sim V}$ measured in these complexes with β_{2d} (72±2 Å,

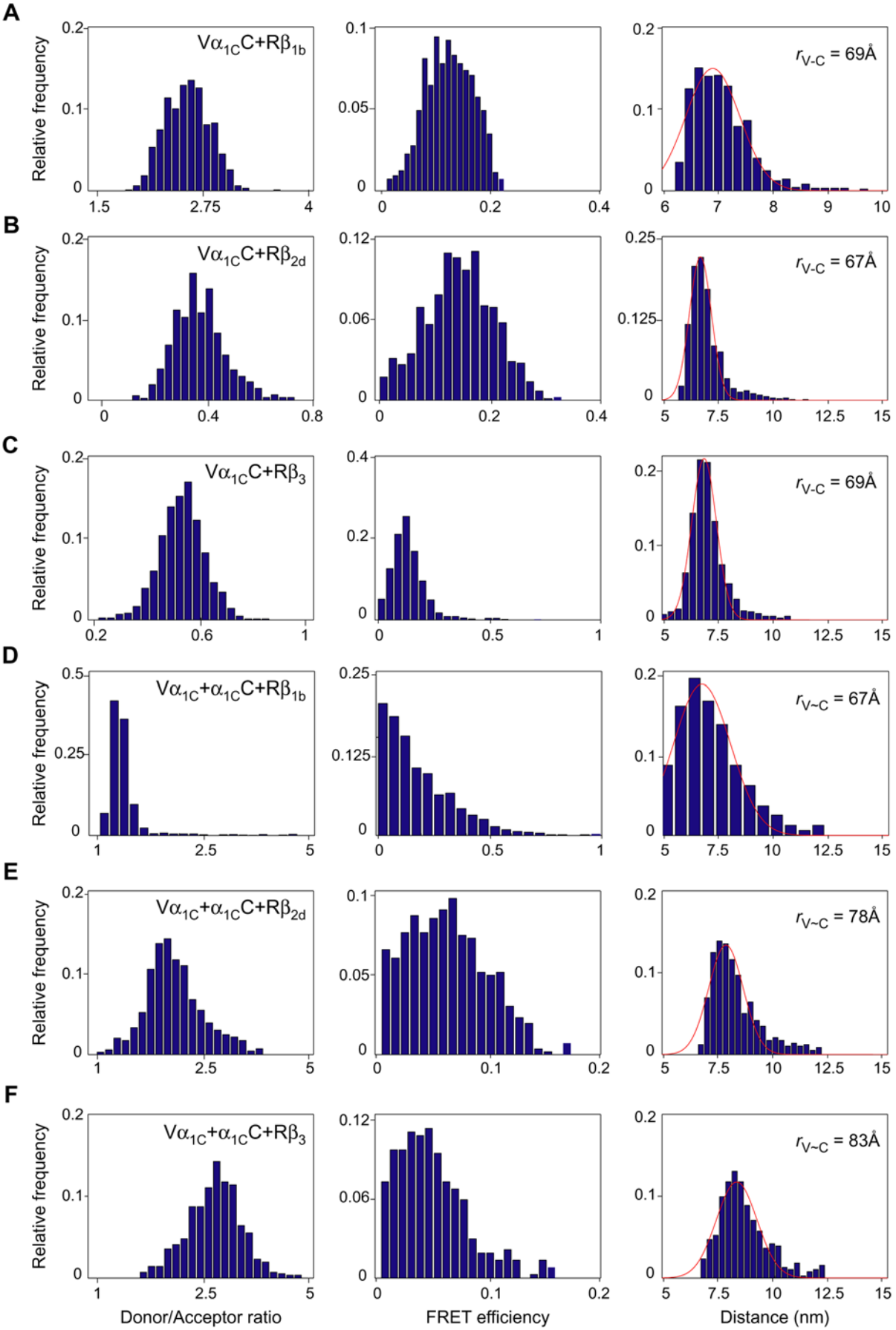
A
Vα1C+Rβ1b
rV-C = 69Å
B
Vα1C+Rβ2d
rV-C = 67Å
C
Vα1C+Rβ3
rV-C = 69Å
D
Vα1C+α1C+Rβ1b
rV~C = 67Å
E
Vα1C+α1C+Rβ2d
rV~C = 78Å
F
Vα1C+α1C+Rβ3
rV~C = 83Å
Relative frequency
Donor/Acceptor ratio
FRET efficiency
Distance (nm)

Figure 4. Estimation of distance *r* between fluorophores fused to the N- and/or C-termini of the α_{1C} subunit. (*A–C*) Intramolecular FRET recorded with $V\alpha_{1C}C$. (*D–F*) Intermolecular FRET recorded with $V\alpha_{1C}+\alpha_{1C}C$. Channels were co-expressed in COS1 cells with $\alpha_2\delta$ and $R\beta_{1b}$ (*A* and *D*), $R\beta_{2d}$ (*B* and *E*) or $R\beta_3$ (*C* and *F*). Shown are representative of histograms calculated from single exemplary cells for donor/acceptor ratio (left column), FRET efficiency (middle column) and distance (right column). Relative frequency was calculated for total number of pixels in ROI as described in Methods. The red solid line is the best fit to a Gaussian distribution with indicated means for $r_{V\text{-}C}$ and $r_{V\sim C}$.
doi:10.1371/journal.pone.0005587.g004

Table 1. Intra- and intermolecular distances between the $Ca_v1.2$ calcium channel α_{1C} and β subunits measured by three-color FRET microscopy.

Channel subunits	Measured distances (*r*)	β_{1b}	β_{2d}		β_3	
		r, Å	*r*, Å	*c*	*r*, Å	*c*
$V\alpha_{1C}C+R\beta$	$r_{C\text{-}V}$	68±1 (17)	68±2 (13)	0.90±0.37	69±1 (19)	0.60±0.05
	$r_{C\sim V}$		72±3 (5)	1.27±0.54	77±3 (6)	1.16±0.17
	$r_{V\text{-}R}$	95±3 (13)	99±3§ (8)	1.70±0.27	90±2 (19)	0.97±0.20
	$r_{V\sim R}$		107±1 (3)	2.52±0.17	100±2 (15)	1.72±0.23
	$r_{C\text{-}R}$	85±2‡ (13)	84±2 (13)		79±1 (14)	0.70±0.10
	$r_{C\sim R}$				85±1 (10)	1.55±0.07
$V\alpha_{1C}+\alpha_{1C}C+R\beta$	$r_{C\sim V}$	67±1* (26)	72±2 (13)		79±4 (10)	
	$r_{V\text{-}R}$	90±2 (26)	90±2 (13)		90±5 (10)	
	$r_{C\text{-}R}$	78±1† (26)	86±2 (6)		80±4 (8)	

*$P<0.002$ vs. β_3.
†$P<0.05$ vs. β_{2d}.
‡$P<0.05$ vs. β_3.
§$P<0.05$ vs. $r_{V\text{-}R}$ in $V\alpha_{1C}+\alpha_{1C}C+R\beta_{2d}$.
FRET efficiency between the indicated fluorophores fused to the α_{1C} and β_{1b}, β_{2d} or β_3 subunits was measured in the plasma membrane of expressing COS1 cells and fitted to a Gaussian function. In cases when the routine curve fit showed two significantly different Gaussian distributions, the corresponding dispersion coefficients *c* (mean±SEM) are shown for both distances (see Experimental Procedures). V – mVenus, C- mCerulean, R – tagRFP. Shown values of *r* are mean±SEM. Number of cells is shown in parentheses.
doi:10.1371/journal.pone.0005587.t001

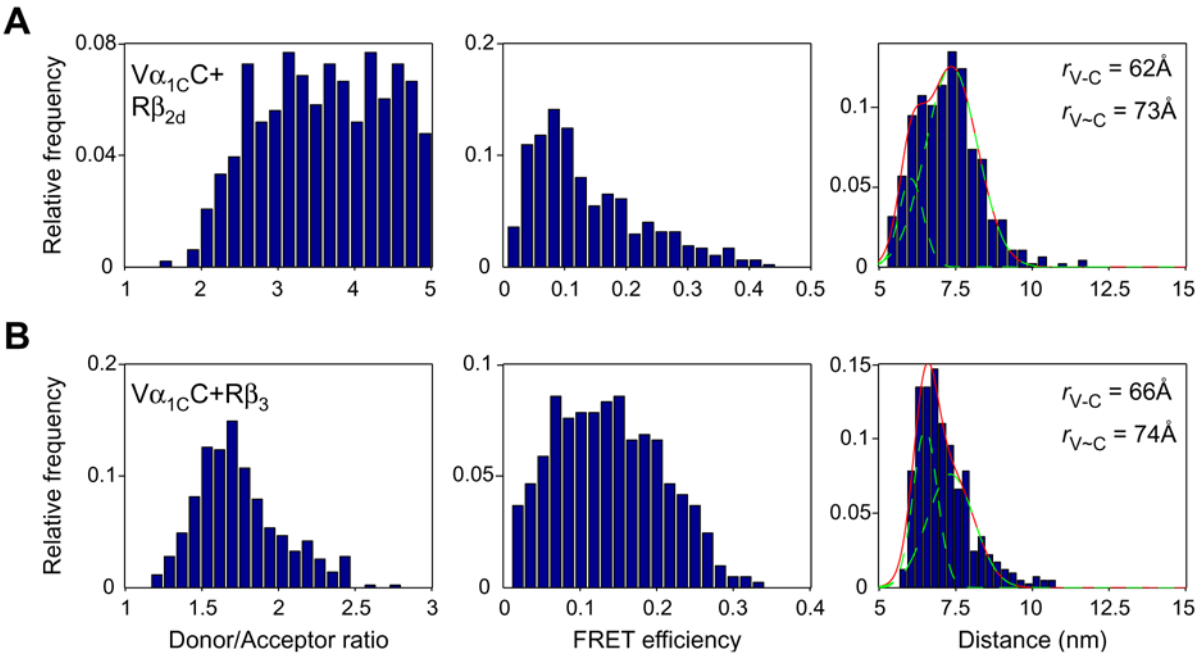

Figure 5. Intramolecular vs. intermolecular FRET in $V\alpha_{1C}C$. The $V\alpha_{1C}C$ subunit was co-expressed in COS1 cells with $\alpha_2\delta$ and $R\beta_{2d}$ (*A*) or $R\beta_3$ (*B*). Shown are histograms of donor/acceptor ratio (left column), FRET efficiency (middle column) and distance (right column) determined in the plasma membrane region of two representative COS1 cells. The red solid line is the best fit to a sum of two Gaussian distributions with indicated means (green dotted lines) for intramolecular ($r_{C\text{-}V}$) and intermolecular FRET ($r_{C\sim V}$).
doi:10.1371/journal.pone.0005587.g005

n = 13) and β_3 (79±4 Å, n = 10) are not significantly different from the $r_{C\sim V}$ values measured under the same conditions with $V\alpha_{1C}C$. With β_{1b}, the intermolecular distance $r_{C\sim V}$ measured between $V\alpha_{1C}$ and $\alpha_{1C}C$ was 67±1 Å (n = 26), a value not significantly different from the estimate for intramolecular $V\alpha_{1C}C$ distance ($r_{V\text{-}C}$ = 68±1 Å, n = 17). This explains why the data obtained in the presence of β_{1b} were best fitted by a single Gaussian distribution. Thus, unlike β_{2d} and β_3, in the presence of β_{1b} the inter- and intramolecular distances appear to be similar.

The measurements with a mixture of $V\alpha_{1C}$ and $\alpha_{1C}C$ confirm that $Ca_v1.2$ calcium channels containing β_{1b}, β_{2d} or β_3 subunits are in close proximity to each other, thus supporting their clustering in the plasma membrane. The distance $r_{C\sim V}$ between the N- and C-termini of the neighbor α_{1C} subunits depends on the type of $Ca_v\beta$. In the presence of β_{1b}, the distance $r_{C\sim V}$ (67±1 Å) is 1.2 nm smaller ($P<0.002$) than with β_3 (79±4 Å), while $r_{C\sim V}$ estimated in the presence of β_{2d} (72±2 Å) is of an intermediate value. Subsequent measurements of three-color FRET between $R\beta$ and the fluorophores of the α_{1C} subunit added more certainty to this general picture (Figure 6*A*).

FRET between tagRFP-labeled $Ca_v\beta$ and mCerulean/mVenus-labeled α_{1C}

The three $Ca_v\beta$ subunits selected for our study vary in molecular mass (β_{1b}, 53.2 kDa; β_{2d}, 73.5 kDa; β_3, 54.5 kDa) and in the size of the variable N-terminal (V1), central (HOOK) and C-terminal (V2) regions (see Figure 6*B*). There are large differences between the three $Ca_v\beta$ subunits in variable regions on both sides of the AID-binding pocket, which anchors $Ca_v\beta$ to the I–II linker of α_{1C} (Figure 6*A*). In spite of that, the intramolecular distance $r_{V\text{-}R}$ between $R\beta$ and $V\alpha_{1C}$ estimated in all tested three-color FRET combinations, including single- or double-labeled α_{1C} ($V\alpha_{1C}$+$\alpha_{1C}C$+$R\beta$, $V\alpha_{1C}C$+$R\beta$), was not significantly different for all tested $Ca_v\beta$ subunits except for $R\beta_{2d}$ (see § in Table 1) Although the average distances $r_{C\text{-}R}$ between $R\beta$ and $V\alpha_{1C}C$ were significantly different for $R\beta_{1b}$ (85±2 Å, n = 13) and $R\beta_3$ (79±1 Å, n = 14), they were not significantly different between $R\beta$ and $\alpha_{1C}C$. A superposition of all three simultaneously measured arrangements between $R\beta$ and $V\alpha_{1C}C$ (Figure 6*C*) illustrates differences in the positions of $R\beta$ subunits as reflected by statistically significant differences in $r_{V\text{-}R}$ and $r_{C\text{-}R}$ (Table 1).

Fitting to a sum of two Gaussian distributions did not reveal the second (intermolecular) component of FRET between $V\alpha_{1C}C$ and $R\beta_{1b}$ (Table 1). However in the case of $R\beta_3$ two intermolecular FRET components were clearly observed, one corresponding to the distance $r_{V\sim R}$ = 100±2 Å (in 15 of 19 cells) and the other corresponding to $r_{C\sim R}$ = 85±1 Å (in 10 of 14 cells). In the presence of $R\beta_{2d}$, the latter component was not observed (n = 13), suggesting that the related distance $r_{C\sim R}$ exceeded 102 Å. However, intermolecular FRET between $V\alpha_{1C}$ and $R\beta_{2d}$ was distinctly revealed in 3 out of 8 cells in a range close to the limits of resolution of the method with an estimate of $r_{V\sim R}$ = 107±1 Å (Table 1). Taken together, FRET measurements between $R\beta$ and the labeled tails of $V\alpha_{1C}C$ corroborated data on intermolecular FRET obtained with $V\alpha_{1C}$+$\alpha_{1C}C$+$R\beta$ and demonstrated that (a) calcium channels are in close proximity in the plasma membrane, and (b) both the intra- and intermolecular architecture of $Ca_v1.2$ channels depend on the type of $Ca_v\beta$ present.

Discussion

$Ca_v1.2$ calcium channels initiate Ca^{2+} signal transduction to many different downstream targets in wide variety of cells. Investigation of factors affecting structural organization of $Ca_v1.2$ channels is crucial for better understanding the mechanisms of Ca^{2+} signaling. The tendency of $Ca_v1.2$ channels to form clusters in the plasma membrane of different cell types has been poorly investigated. Here we studied effects of three major $Ca_v\beta$ subunits on structural organization of recombinant $Ca_v1.2$ channels expressed in COS1 cells. Because untransfected COS1 cells do not express endogenous calcium channels, they lack natural intracellular partners (e.g., cardiac RyR2) in proximity of exogenous $Ca_v1.2$ channels that might promote their clustering through "junctional" coupling [45]. However, recombinant $Ca_v1.2$ channels expressed in COS1 cells establish functional coupling to CREB-dependent transcriptional activation [46], pointing to a physiologically relevant integration of recombinant $Ca_v1.2$ into a naturally occurring signaling cascade with Ca^{2+}/calmodulin-dependent protein kinase II mediating this activity in native cells [47].

TIRF microscopy revealed clusters of recombinant $Ca_v1.2$ channels in the plasma membrane of COS1 cells. The size and the plasma membrane density of the clusters significantly depend on the type of $Ca_v\beta$ present. This important observation suggests that the type of $Ca_v\beta$ present determines the structure of the $Ca_v1.2$ clusters. The average cluster size varies from 360 (β_{1b}) to 450 nm^2 (β_3). Corroborating reasonable dimensions of these values, a mean size of the $Ca_v1.2$ cluster with the major cardiac β_{2d} (430 nm^2) is within the estimated size range (250–560 nm^2) of rat ventricular RyR2 clusters [48].

Relative arrangement of α_{1C} and $Ca_v\beta$ was estimated with sub-nanometer precision using three-color FRET microscopy in live cells with calcium channels in a stable, inactivated state. Our study revealed that in spite of substantial differences in molecular structure (Figure 6*B*), the intramolecular distance between the α_{1C} subunit tails does not significantly depend on the type of $Ca_v\beta$ present. Relative position of $R\beta_{1b}$, $R\beta_{2d}$ and $R\beta_3$ did not differ significantly. This is interesting because, unlike β_{1b} and β_3, β_{2d} has a C-terminal β_2CED domain, which interacts with the IQ region of the α_{1C} C-tail [44].

Another important observation is that N- and C-termini of α_{1C} and N-termini of $Ca_v\beta$ subunits of neighbor channels are in close (<120 Å) proximity to each other, which corroborates with the tendency of $Ca_v1.2$ to form clusters. Intermolecular distance between the α_{1C} subunits significantly depends on the type of $Ca_v\beta$ and increases from 67 Å in the presence of β_{1b} to 79 Å with β_3. Measurements of FRET between $R\beta$ and neighbor V/C-α_{1C} supported this general picture and showed a significant effect of the type of $Ca_v\beta$ present on the relative position of neighbor channels.

Interestingly, freeze-fracture of the surface membrane revealed that distances between $Ca_v1.2$ channels trapped in cardiac junctions with RyR2 is variable and, on average, are larger than those identified by FRET [49]. It is known that the cytoskeleton and RyR2 associate with $Ca_v1.2$ plasma membrane clusters in heart cells [50]. Thus, one can not exclude that the distance between $Ca_v1.2$ channels in clusters in cardiac junctions is affected by RyR2. However, it is not clear whether clustering affects the ability of $Ca_v1.2$ channels to initiate Ca^{2+} signaling and whether every channel is responsive to depolarizing stimuli. In cardiac muscle cells, a single $Ca_v1.2$ opening triggers activity of 4–6 RyR2 [51]. The average size of a RyR2 cluster in ventricular myocytes plasma membrane is 250 nm^2 (~100 RyR2 molecules) [48] and interaction between $Ca_v1.2$ and RyR2 is weaker than that between $Ca_v1.1$ and RyR1 in skeletal muscle. Thus, activation of a RyR2 cluster may be mediated by random opening of few $Ca_v1.2$ channels in clusters located at a larger distance than that estimated by FRET.

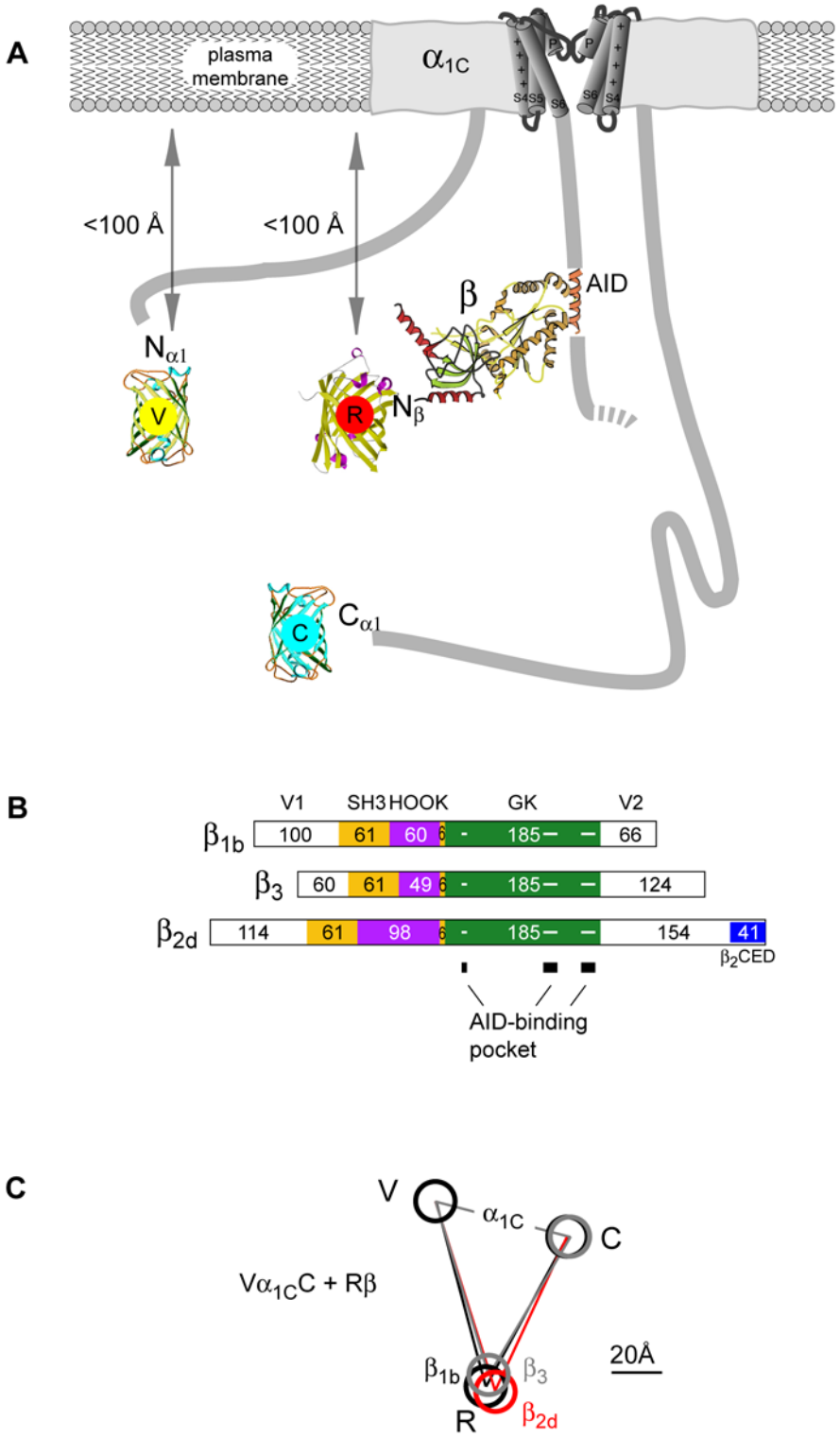

Figure 6. Molecular distances between the N- and C-termini of α_{1C} and the $Ca_v\beta$-subunit N-tail of β_{1b}, β_{2d} and β_3. (*A*) Schematic representation of $V\alpha_{1C}C$ with $R\beta$ arranged under a vertically sliced α_{1C}. The structures of TagRFP and $Ca_v\beta$ core MAGUK region were drawn based on PDB codes 1uisA [37] and 1t0j [62], respectively. FRET measurements with ECFP-labeled plekstrin homology domain in the inner leaflet of the plasma membrane [40,63] showed that the N terminal tags of both the α_{1C} and $Ca_v\beta$ subunits are located within the 2× Förster distance (<100 Å for ECFP/EYFP) from the plasma membrane. (*B*) Schematic representation of the domain organization of β_{1b}, β_{2d} and β_3 aligned in regard to AID-binding guanylate kinase (GK) domain (green). Yellow box indicates the Src homology 3 (SH3) domain, purple the variable HOOK region, and blue the β_2CED [44]. Number of amino acids is shown inside boxes. Amino acids involved in AID-binding pocket are marked in GK by three horizontal lines (for details see [62,64,65]). (*C*) Schematic representation of the results of simultaneous measurements of the molecular distances between three fluorophores shown in panel (*A*) in $V\alpha_{1C}C/\alpha_2\delta/R\beta$ in the presence of $R\beta_{1b}$ (black lines), $R\beta_3$ (gray lines) and $R\beta_{2d}$ (red lines).
doi:10.1371/journal.pone.0005587.g006

Little is known about molecular determinants underlying physiologically important cluster organization of $Ca_v1.2$ channels in neurons [52]. It was shown recently that scaffolding proteins (AKAP79/150 and PDZ) participating in organizing plasma membrane signaling complexes in neurons were not responsible for organizing $Ca_v1.2$ channel clusters [53]. The involvement of $Ca_v\beta$ in $Ca_v1.2$ channel cluster organization, identified in our study, does not contradict the earlier report that the calmodulin-binding IQ region of α_{1C} has a role in $Ca_v1.2$ clustering [19]. Because $Ca_v\beta$s interact with IQ [23,44], it is possible that both act as concerted determinants in $Ca_v1.2$ channel clustering.

In conclusion, our study revealed effects of $Ca_v\beta$ subunits on the structural organization of $Ca_v1.2$ calcium channel in the plasma membrane in the absence of "junctional" interactions. It remains to be seen whether the observed differences in the cluster packing and arrangement of $Ca_v1.2$ contribute to the observed differences in calcium signaling among the cell types with preferential expression of a certain type of $Ca_v\beta$ [54–56].

Materials and Methods

Labeling α_{1C} subunit with mVenus and/or mCerulean

To avoid dimerization, only monomeric forms of fluorescent proteins were used. The C-terminus of human $Ca_v1.2$ calcium channel $\alpha_{1C,77}$ subunit was amplified by PCR with sense 5′-ctattgaattcgatatcTGCCAGCAGCCTGGTGGAAGCG-3′ and antisense 5′-gtattaccggtggCAGGCTGCTGACGTAGACCCTGC-3′ primers. The PCR fragment was cleaved with ECoRI and AgeI and incorporated into an mCerulean-N1 [57] vector cleaved with the same enzymes, and the 5′-ECoRV/NotI-3′ fragment from the resulting plasmid was then incorporated into $\alpha_{1C,77}$-pCDNA3 cleaved with AleI and NotI, resulting in the $mCerulean_C$-$\alpha_{1C,77}$-pCDNA3 plasmid coding for α_{1C}C. The 5′-NdeI/KpnI-3′ fragment from mVenus-C1 vector [26] was incorporated into $\alpha_{1C,77}$-pCDNA3 and $mCerulean_C$-$\alpha_{1C,77}$-pCDNA3 cleaved with the same enzymes to yield $mVenus_N$-$\alpha_{1c,77}$-pCDNA3 and $mVenus_N$-$mCerulean_C$-$\alpha_{1c,77}$-pCDNA3, respectively, coding for Vα_{1C} and Vα_{1C}C.

Labeling of $Ca_v\beta$ subunits with monomeric fluorescent tags

The cDNA of human β_{1b} and β_3 subunits was cloned from a human heart mRNA (Promega) by a nest RT-PCR strategy. For β_{1b}, 5′-GACGGGCAGGGCGCCCACTAC-3′ was used as primer for the reverse transcription, sense 5′-GAGGCTCCTCTCCA-TGGTCCAG-3′ and antisense 5′-CCACTACATGGCATGT-TCCTGC-3′ primers were used for the first round PCR, sense 5′-GCCACCATGGTCCAGAAGACCAG-3′ and antisense 5′-CAC-TACATGGCATGTTCCTGCTC-3′ primers were used for the second round PCR. For β_3, primer 5′-CGCCTGTGCCT-GCCAGGGTAGGGCAGCAGG-3′ was used for the reverse transcription, sense 5′-GACTCCCCCATGTATGACGAC-3′ and antisense 5′-GGCTGTCAGTAGCTATCCTTG-3′ primers were used for the first round PCR, sense 5′-GCCACCATGTAT-GACGACTCC-3′ and antisense 5′-TGTCAGTAGCTATC-CTTGGGC-3′ primers were used for the second round PCR. The cDNA was cloned into a TA cloning vector pCR 2.1 (Invitrogen) and confirmed by DNA sequencing. The 5′-EcoRV/BamHI-3′ fragment of a β_{1b} TA clone was incorporated into the pTagRFP-C vector (Evrogen, Moscow, Russia), which was cleaved with XhoI, filled in with Klenow and then cleaved with BamHI to generate RFP-β_{1b} (Rβ_{1b}). In a similar way the 5′-XhoI/HindIII-3′ fragment of a β_3-TA clone was incorporated into the pTagRFP-C vector to generate monomeric Rβ_3. To prepare RFP-β_{2d}, β_{2d} was amplified by PCR using mVenus-β_{2d} [44] as template with sense primer 5′-CGGAGATCTATGGTCCAAAGGGACATGTC-3′ and antisense primer 5′-GGGGTCGACTCATTGGGGGATG-TAAACATC-3′, and then the PCR product was cleaved with BglII and SalI, and incorporated into the pTagRFP-C vector cleaved with the same enzymes.

FRET calibration constructs

CTV, C5V, C39V, CVC and VCV were obtained from Drs. Ikeda and Vogel (NIAAA, NIH). The 5′-NheI/BsrGI:(Klenow-filled-in)-3′ fragments of mVenus-C1 and mCerulean-C1 were cloned into pTagRFP-C, which was cleaved with AgeI, filled in with Klenow and then cleaved with NheI, to make V4R and C4R respectively. The 5′-NheI/BamHI:(Klenow-filled-in)-3′ fragment of pTagRFP-C was cloned into mCerulean-N1, which was cleaved with EcoRI, filled in with Klenow and then cleaved with NheI, to make R39C. To prepare R17V and R17C, the 5′-NheI/XhoI:(Klenow-filled-in)-3′ fragment of pTagRFP-C was cloned, respectively, into mVenus-N1 and mCerulean-N1, which were cleaved with BamHI (Klenow filled in) and NheI. CTV was cleaved with BspEI, and the 0.7 Kb fragment was inserted into R17V and R17C to generate RTV and RTC, respectively. mCerulean was amplified by PCR using sense primer 5′-TATATCCGGAGATATCATGGTGAGCAAGGGCGAGGAG-3′ and antisense primer 5′-TATAGAATTCTTTGTACAGCTCG-TCCATGCCGA-3′. After cleavage with BspEI and EcoRI, the PCR product of mVenus was inserted into pTagRFP-C to yield R5V; the PCR product of mCerulean was inserted into pTagRFP-C and C4R to yield R5C and CRC, respectively. RFP was amplified by PCR with sense primer 5′-TATAGAATTCGATATCATG-GTGTCTAAGGGCGAAGAGCTG-3′ and antisense 5′-ATATG-GTACCATTAAGTTTGTGCCCCAGTTTGCTAG-3′, cleaved with EcoRI and KpnI, and incorporated into R5V and R5C cleaved with the same enzymes to yield RVR and RCR, respectively.

Imaging

Images were recorded with a pixel size of ca. 200 nm using a 14-bit Hamamatsu C9100-12 digital camera (Hamamatsu City, Japan) mounted on a Nikon TE2000 epifluorescent microscope (Tokyo, Japan) equipped with a 60×1.45 numerical aperture (n.a.) oil objective and multiple filter sets (Chroma Technology, Rockingham, VT). Excitation light was delivered by a 175 W xenon lamp. Excitation filter sets were changed by a high-speed filter wheel system (Lambda 10-2, Sutter Instrument, Novato, CA). The Dual-View system (Optical Insights, Santa Fe, NM) was used for the simultaneous acquisition of two fluorescence images (donor and FRET). Images were collected and analyzed using C-Imaging (Compix, Cranberry Township, PA) and MATLAB v.7.0.4 (The Mathworks, Natick, MA).

Two-color FRET was quantified with three filter sets: for the yellow fluorescent protein (YFP) cube, excitation filter 500/20 nm, dichroic beam splitter 515 nm, emission filter 535/30 nm; for the cyan fluorescent protein (CFP) cube, excitation filter 436/20 nm, dichroic beam splitter 505 nm, emission filter 480/40 nm; for the FRET cube (CFP/YFP), excitation filter 436/20 nm, dichroic beam splitter 5051nm, emission filter 540/30 nm. For three-color FRET, the six-filter method described in [39] was used. All FRET images were acquired sequentially. For imaging mCerulean/mVenus pairs, the same filter arrangement as for two-color FRET was used. For the mCerulean/tagRFP combination, the following settings were used: for CFP cube, excitation filter 436/20 nm, dichroic beam splitter 505 nm, emission filter 480/40 nm; for RFP cube, excitation filter 555/28 nm, dichroic beam splitter 565 nm, emission filter 630/50 nm; for the FRET cube, excitation filter 436/20 nm, dichroic beam splitter 565 nm, emission filter 630/50 nm. With the mVenus/tagRFP combination, the following filter arrangement was used: for

YFP cube, excitation filter 500/20 nm, dichroic beam splitter 515 nm, emission filter 535/30 nm; for RFP cube, excitation filter 555/28 nm, dichroic beam splitter 565 nm, emission filter 630/50 nm; for the FRET cube, excitation filter 484/15, dichroic beam splitter 565 nm, emission filter 630/50 nm. TIRF images were obtained with TIRF2 Nikon system mounted on Nikon TE2000 microscope and argon-ion laser with 514 nm line and diode laser with 440 nm line, dichroic beam splitter 505 nm, emission filters 470/30 nm and 550/30 nm.

Clusters within TIRF images were identified using 2D continuous wavelet transform similar to [58]. Images were analyzed using a two-dimensional mexican hat wavelet over scales 0.5 through 2 to identify ROI of locally increased signal fluorescence up to 5 μm^2 in area. Similar approaches have been employed for cluster detection in clinical and cell biology imaging [46,59,60]. Corrected FRET intensity was calculated from data acquired using the three filter sets (CFP, YFP, and FRET) as described previously [40] using MATLAB. Briefly, corrected FRET values ($FRET_c$) were calculated according to

$$FRET_c = I_{FRET} - aI_d\text{-}bI_a,$$

where a and b are bleedthrough coefficients and I_{FRET}, I_d and I_a are FRET, donor and acceptor intensities.

Measurement of the G factor, which relates the increase in sensitized acceptor emission to the loss of donor fluorescence (quenching), is critical for calculating FRET efficiency (E) using the three-filter cube method. G factor is a constant for a particular fluorophore pair and imaging setup [42]. This method requires preparation of cDNA constructs encoding donor-acceptor fusion fluorescent proteins differing as widely as possible in FRET efficiency. This was accomplished by varying the length and composition of the linker residues connecting mCerulean and mVenus, mCerulean and tagRFP or mVenus and tagRFP. G factor was determined as

$$G = \frac{F_{c1}/I_{aa1} - F_{c2}/I_{aa2}}{I_{dd2}/I_{aa2} - I_{dd1}/I_{aa1}},$$

where I_{aa1}, I_{dd1} and F_{c1} are acceptor, donor and corrected FRET intensity of the construct with the shortest linker between donor and acceptor, and I_{aa2}, I_{dd2} and F_{c2} are acceptor, donor and corrected FRET intensity of the construct with the longest linker between donor and acceptor. Using this formula, we found G factors of 1.81 for the mCerulean/mVenus pair, 1.30 for the mVenus/tagRFP pair, and 0.38 for the mCerulean/tagRFP pair. These G factor values allowed us to calculate FRET efficiency according to [42] as follows:

$$E = \frac{F_c/G}{I_{dd} + F_c/G}$$

The distance between two fluorophores was calculated in accordance with Förster theory:

$$r = \sqrt[6]{R_0^6 \frac{1-E}{E}}$$

The Förster distances (R_0), the characteristic distance where the FRET efficiency is 50%, was calculated according to [61]:

$${R_0}^6 = C\kappa^2\eta^{-4}Q_D\varepsilon_A J(\lambda),$$

where Q_D is the donor quantum yield, ε_A is the maximal acceptor extinction coefficient, and $J(\lambda)$ is the spectral overlap integral between the normalized donor fluorescence and the acceptor excitation spectra. All these parameters were calculated based on data obtained from Evrogen for tagRFP and reported for mCerulean and mVenus in [61]. Other parameters included coefficient $C = 8.786\times10^{-11}$ mol$\oplus$L$^{-1}\oplus$cm$\oplus$nm^2, $\kappa^2 \leq 2/3$ representing the angle between the two fluorophore dipoles assuming random orientation, and $\eta \leq 1.4$, the typical refractive index for biomolecules in aqueous solution [43]. The Förster distance estimated for mCerulean-mVenus was 5.3 nm, while R_0 for mCerulean-tagRFP was 5.1 nm and R_0 for mVenus-tagRFP was 5.8 nm. The k factor - the ratio of donor to acceptor (D/A) fluorescence intensity for equimolar concentrations in the absence of FRET, was determined for each construct in accordance with [42]:

$$k = \frac{I_{dd} + F_c/G}{I_{aa}}$$

The k factor for mCerulean/mVenus was calculated to be 0.41, while mVenus/tagRFP gave $k = 1.60$ and mCerulean/tagRFP gave $k = 0.27$.

D/A ratio for arbitrary concentrations of donor and acceptor was calculated according to [42]:

$$D/A = \frac{I_{dd} + F_c/G}{I_{aa}k}$$

For corrected FRET efficiency measurements, this ratio should be in the range from 0.2 to 5.0 [41]. During analysis, the pixels with D/A ratio outside this range were eliminated from the FRET efficiency calculations.

Validation of G and k factors is presented in Figure S1 for two- and three-color FRET standards with different FRET efficiencies (linkers) and D/A stoichiometry. In our three-color FRET experiments, the major energy transfer was observed directly between mCerulean and tagRFP and not from cascade transfer through mVenus. If there would be a significant contribution of cascade FRET through mVenus, we would see a decrease in efficiency when we used two-color FRET (mCerulean/tagRFP) compared with three-color FRET, potentially including contributions from mCerulean/mVenus/tagRFP cascade. We did not observe a decrease in efficiency with two-color FRET, as experiments with Rβ_3 and α_{1C}C gave the same efficiency of 0.05 ($r = 80$ nm) as three-color FRET experiments with Rβ_3, α_{1C}C and Vα_{1C}. Additional control experiments showed that the third fluorophore did not have a significant effect on mCerulean-mVenus FRET: we did not observe a significant difference between the distance between mCerulean/mVenus fluorophores (73 ± 3, n = 10) measured by two-color FRET with Vα_{1C}C and unlabeled β_{2d} and that obtained with three-color FRET using Rβ_{2d} and Vα_{1C}C (68 ± 2 nm, n = 13).

For each cell, we calculated FRET efficiency and distances (r) between fluorophores in each pixel of ROI. Gaussian fitting of the r distribution (20 bin histogram) was done in MATLAB using the fit function:

$$f(r) = ae^{-\left(\frac{r-b}{c}\right)^2},$$

where b is the position of the center of the peak (mean) and c (dispersion coefficient) reflects the width of the distribution.

Supporting Information

Figure S1 FRET efficiency and donor/acceptor ratio of FRET standards. Shown are bar graphs summarizing the mean FRET efficiency (A) and the D/A ratio (B) for the indicated FRET calibration constructs. Data are presented as mean±SEM. (A) FRET efficiency values were: C4R (0.110±0.005), R39C (0.081±0.003), CTV (0.023±0.004), V4R (0.433±0.011), RTV (0.191±0.009), C5V (0.474±0.014), C39V (0.266±0.014) and CTV (0.179±0.006). (B) D/A ratios were: C4R (0.99±0.009), R39C (1.00±0.10), RTC (1.00±0.06), CRC (1.96±0.10), RCR (0.48±0.03), V4R (1.00±0.07), RTV (1.00±0.10), RVR (0.53±0.09), C5V (1.00±0.04), C39V (0.95±0.09), CTV (1.00±0.06), CVC (2.00±0.10) and VCV (0.54±0.02). The number of tested cells is shown in the bars. As one can see, increasing the length of the linker between the fluorophores significantly reduced FRET efficiency consistent with an increased distance between donor and acceptor. The measured mean D/A ratio corresponds well to the expected values of 1.0 (1:1), 2.0 (2:1) and 0.5 (1:2). D/A ratios were also determined for the three-color construct CRV. D/A ratio and FRET efficiency were calculated in CRV independently for each pair of fluorophores. D/A ratio (E_{FRET}) are: for CV, 1.00±0.07 (0.45±0.02); for VR, 1.10±0.10 (0.41±0.02), and for CR, 0.99±0.07 (0.20±0.01), n = 11. Thus, the D/A ratio of three-color standards well corresponds to the expected 1:1 ratio.
Found at: doi:10.1371/journal.pone.0005587.s001 (0.29 MB EPS)

Acknowledgments

The authors thank Dr. Stephen R. Ikeda and Dr. Steven S. Vogel for their gift of mVenus and mCerulean/mVenus fused constructs, and Dr. David W. Piston for his gift of mCerulean. The authors are grateful to Dr. Clara Franzini-Armstrong for critical discussion of the results and to Dr. Kenneth Fishbein for critically reading the manuscript.

Author Contributions

Conceived and designed the experiments: EK NS. Performed the experiments: EK PA. Analyzed the data: EK PA SQD ST. Contributed reagents/materials/analysis tools: JBH CP QZL. Wrote the paper: EK SQD NS.

References

1. Clapham DE (1995) Calcium signaling. Cell 80: 259–268.
2. Lipscombe D, Madison DV, Poenie M, Reuter H, Tsien RY, et al. (1988) Spatial distribution of calcium channels and cytosolic calcium transients in growth cones and cell bodies of sympathetic neurons. Proc Natl Acad Sci USA 85: 2398–2402.
3. Silver RA, Lamb AG, Bolsover SR (1990) Calcium hotspots caused by L-channel clustering promote morphological changes in neuronal growth cones. Nature 343: 751–754.
4. Westenbroek RE, Ahlijanian MK, Catterall WA (1990) Clustering of L-type Ca^{2+} channels at the base of major dendrites in hippocampal pyramidal neurons. Nature 347: 281–284.
5. Franzini-Armstrong C, Protasi F, Ramesh V (1998) Comparative ultrastructure of Ca^{2+} release units in skeletal and cardiac muscle. Ann NY Acad Sci 853: 20–30.
6. Franzini-Armstrong C, Protasi F, Tijskens P (2005) The assembly of calcium release units in cardiac muscle. Ann NY Acad Sci 1047: 76–85.
7. Gathercole DV, Colling DJ, Skepper JN, Takagishi Y, Levi AJ, et al. (2000) Immunogold-labeled L-type calcium channels are clustered in the surface plasma membrane overlying junctional sarcoplasmic reticulum in guinea-pig myocytes-implications for excitation-contraction coupling in cardiac muscle. J Mol Cell Cardiol 32: 1981–1994.
8. Harms GS, Cognet L, Lommerse PHM, Blab GA, Kahr H, et al. (2001) Single-molecule imaging of L-type Ca^{2+} channels in live cells. Biophys J 81: 2639–2646.
9. Hell JW, Westenbroek RE, Warner C, Ahlijanian MK, Prystay W, et al. (1993) Identification and differential subcellular localization of the neuronal class C and class D L-type calcium channel α1 subunits. J Cell Biol 123: 949–962.
10. Takagishi Y, Yasui K, Severs NJ, Murata Y (2000) Species-specific difference in distribution of voltage-gated L-type Ca^{2+} channels of cardiac myocytes. Am J Physiol Cell Physiol 279: C1963–1969.
11. Di Biase V, Franzini-Armstrong C (2005) Evolution of skeletal type e-c coupling: a novel means of controlling calcium delivery. J Cell Biol 171: 695–704.
12. Woo S-H, Soldatov NM, Morad M (2003) Modulation of Ca^{2+} signalling in rat atrial myocytes: possible role of the α_{1C} carboxyl terminal. J Physiol (Lond) 552: 437–447.
13. Shuai JW, Jung P (2003) Optimal ion channel clustering for intracellular calcium signaling. Proc Natl Acad Sci U S A 100: 506–510.
14. Inoue M, Bridge JHB (2003) Ca^{2+} sparks in rabbit ventricular myocytes evoked by action potentials: Involvement of clusters of L-type Ca^{2+} channels. Circ Res 92: 532–538.
15. Pate P, Mochca-Morales J, Wu Y, Zhang J-Z, Rodney GG, et al. (2000) Determinants for calmodulin binding on voltage-dependent Ca^{2+} channels. J Biol Chem 275: 39786–39792.
16. Peterson BZ, DeMaria CD, Adelman JP, Yue DT (1999) Calmodulin is the Ca^{2+} sensor for Ca^{2+}-dependent inactivation of L-type calcium channels. Neuron 22: 549–558.
17. Qin N, Olcese R, Bransby M, Lin T, Birnbaumer L (1999) Ca^{2+}-induced inhibition of the cardiac Ca^{2+} channel depends on calmodulin. Proc Natl Acad Sci USA 96: 2435–2438.
18. Zühlke RD, Pitt GS, Deisseroth K, Tsien RW, Reuter H (1999) Calmodulin supports both inactivation and facilitation of L-type calcium channels. Nature 399: 159–162.
19. Kepplinger KJF, Kahr H, Förstner G, Sonnleitner M, Schneider H, et al. (2000) A sequence in the carboxy-terminus of the α_{1C} subunit important for targeting, conductance and open probability of L-type Ca^{2+} channels. FEBS Lett 477: 161–169.
20. Fallon JL, Baker MR, Xiong L, Loy RE, Yang G, et al. (2009) Crystal structure of dimeric cardiac L-type calcium channel regulatory domains bridged by Ca^{2+}·calmodulins. Proc Natl Acad Sci U S A published online before print March 11, 2009: 1–6.
21. Colecraft HM, Alseikhan B, Takahashi SX, Chaudhuri D, Mittman S, et al. (2002) Novel functional properties of Ca^{2+} channel β subunits revealed by their expression in adult rat heart cells. J Physiol (Lond) 541: 435–452.
22. Varadi G, Lory P, Schultz D, Varadi M, Schwartz A (1991) Acceleration of activation and inactivation by the β subunit of the skeletal muscle calcium channel. Nature 352: 159–162.
23. Zhang R, Dzhura I, Grueter CE, Thiel W, Colbran RJ, et al. (2005) A dynamic α-β inter-subunit agonist signaling complex is a novel feedback mechanism for regulating L-type Ca^{2+} channel opening. FASEB J 19: 1573–1575.
24. Dolphin AC (2003) β Subunits of voltage-gated calcium channels. J Bioenerg Biomembr 35: 599–620.
25. Pragnell M, De Waard M, Mori Y, Tanabe T, Snutch TP, et al. (1994) Calcium channel β-subunit binds to a conserved motif in the I-II cytoplasmic linker of the α_1-subunit. Nature 368: 67–70.
26. Koushik SV, Chen H, Thaler C, Puhl HL III, Vogel SS (2006) Cerulean, Venus, and VenusY67C FRET reference standards. Biophys J 91: L99–101.
27. Powers PA, Liu S, Hogan K, Gregg RG (1992) Skeletal muscle and brain isoforms of a β-subunit of human voltage-dependent calcium channels are encoded by a single gene. J Biol Chem 267: 22967–22972.
28. Takahashi SX, Mittman S, Colecraft HM (2003) Distinctive modulatory effects of five human auxiliary β_2 subunit splice variants on L-type calcium channel gating. Biophys J 84: 3007–3021.
29. Herzig S, Khan IFY, Grundemann D, Matthes J, Ludwig A, et al. (2007) Mechanism of $Ca_v1.2$ channel modulation by the amino terminus of cardiac β_2-subunits. FASEB J 21: 1527–1538.
30. Castellano A, Wei X, Birnbaumer L, Perez-Reyes E (1993) Cloning and expression of a third calcium channel β subunit. J BiolChem 268: 3450–3455.
31. Collin T, Lory P, Taviaux S, Courtieu C, Guilbault P, et al. (1994) Cloning, chromosomal location and functional expression of the human voltage-dependent calcium-channel β3 subunit. Eur J Biochem 220: 257–262.
32. Hullin R, Singer-Lahat D, Freichel M, Biel M, Dascal N, et al. (1992) Calcium channel β subunit heterogeneity: Functional expression of cloned cDNA from heart, aorta and brain. EMBO J 11: 885–890.
33. Murakami M, Yamamura H, Suzuki T, Kang M-G, Ohya S, et al. (2003) Modified cardiovascular L-type channels in mice lacking the voltage-dependent Ca^{2+} channel β3 subunit. J Biol Chem 278: 43261–43267.
34. Papadopoulos S, Leuranguer V, Bannister RA, Beam KG (2004) Mapping sites of potential proximity between the dihydropyridine receptor and RyR1 in muscle using a cyan fluorescent protein-yellow fluorescent protein tandem as a fluorescence resonance energy transfer probe. J Biol Chem 279: 44046–44056.
35. Malo GD, Pouwels LJ, Wang M, Weichsel A, Montfort WR, et al. (2007) X-ray structure of cerulean GFP: A tryptophan-based chromophore useful for fluorescence lifetime imaging. Biochemistry 46: 9865–9873.
36. Merzlyak EM, Goedhart J, Shcherbo D, Bulina ME, Shcheglov AS, et al. (2007) Bright monomeric red fluorescent protein with an extended fluorescence lifetime. Nat Meth 4: 555–557.

37. Wiedenmann J, Vallone B, Renzi F, Nienhaus K, Ivanchenko S, et al. (2005) Red fluorescent protein eqFP611 and its genetically engineered dimeric variants. J Biomed Optics 10: 014003-014001-014007.
38. Zacharias DA, Violin JD, Newton AC, Tsien RY (2002) Partitioning of lipid-modified monomeric GFPs into membrane microdomains of live cells. Science 296: 913–916.
39. Galperin E, Verkhusha VV, Sorkin A (2004) Three-chromophore FRET microscopy to analyze multiprotein interactions in living cells. Nat Meth 1: 209–217.
40. Kobrinsky E, Kepplinger KJF, Yu A, Harry JB, Kahr H, et al. (2004) Voltage-gated rearrangements associated with differential β-subunit modulation of the L-type Ca^{2+} channel inactivation. Biophys J 87: 844–857.
41. Berney C, Danuser G (2003) FRET or no FRET: A quantitative comparison. Biophys J 84: 3992–4010.
42. Chen H, Puhl HL 3rd, Koushik SV, Vogel SS, Ikeda SR (2006) Measurement of FRET efficiency and ratio of donor to acceptor concentration in living cells. Biophys J 91: L39–41.
43. Lakowicz JR (2006) Principles of Fluorescence Spectroscopy. New York: Springer.
44. Lao QZ, Kobrinsky E, Harry JB, Ravindran A, Soldatov NM (2008) New determinant for the $Ca_v\beta_2$ subunit modulation of the $Ca_v1.2$ calcium channel. J Biol Chem 283: 15577–15588.
45. Protasi F, Sun XH, Franzini-Armstrong C (1996) Formation and maturation of the calcium release apparatus in developing and adult avian myocardium. Dev Biol 173: 265–278.
46. Mager DE, Kobrinsky E, Masoudieh A, Maltsev A, Abernethy DR, et al. (2007) Analysis of functional signaling domains from fluorescence imaging and the two-dimensional continuous wavelet transform. Biophys J 93: 2900–2910.
47. Wheeler DG, Barrett CF, Groth RD, Safa P, Tsien RW (2008) CaMKII locally encodes L-type channel activity to signal to nuclear CREB in excitation-transcription coupling. J Cell Biol 183: 849–863.
48. Chen-Izu Y, McCulle SL, Ward CW, Soeller C, Allen BM, et al. (2006) Three-dimensional distribution of ryanodine receptor clusters in cardiac myocytes. Biophys J 91: 1–13.
49. Sun XH, Protasi F, Takahashi M, Takeshima H, Ferguson DG, et al. (1995) Molecular architecture of membranes involved in excitation-contraction coupling of cardiac muscle. J Cell Biol 129: 659–671.
50. Scriven DRL, Klimek A, Lee KL, Moore EDW (2002) The molecular architecture of calcium microdomains in rat cardiomyocytes. Ann NY Acad Sci 976: 488–499.
51. Wang S-Q, Song L-S, Lakatta EG, Cheng H (2001) Ca^{2+} signalling between single L-type Ca^{2+} channels and ryanodine receptors in heart cells. Nature 410: 592–596.
52. Vacher H, Mohapatra DP, Trimmer JS (2008) Localization and targeting of voltage-dependent ion channels in mammalian central neurons. Physiol Rev 88: 1407–1447.
53. Di Biase V, Obermair GJ, Szabo Z, Altier C, Sanguesa J, et al. (2008) Stable membrane expression of postsynaptic $Ca_v1.2$ calcium channel clusters is independent of interactions with AKAP79/150 and PDZ proteins. J Neurosci 28: 13845–13855.
54. Bers DM (2008) Calcium cycling and signaling in cardiac myocytes. Annu Rev Physiol 70: 23–49.
55. Calin-Jageman I, Lee A (2008) Ca_v1 L-type Ca^{2+} channel signaling complexes in neurons. J Neurochem 105: 573–583.
56. Floyd R, Wray S (2007) Calcium transporters and signalling in smooth muscles. Cell Calcium 42: 467–476.
57. Rizzo MA, Piston DW (2005) High-contrast imaging of fluorescent protein FRET by fluorescence polarization microscopy. Biophys J 88: L14–16.
58. Kammermeier P (2006) Surface clustering of metabotropic glutamate receptor 1 induced by long Homer proteins. BMC Neurosci 7: 1.
59. Lee KL, Orr M, Lithgow B. A Novel Wavelet-Statistics Based Feature Detection System for Detecting Microcalcifications; 2005, 7664–7667.
60. Papadopoulos A, Fotiadis DI, Costaridou L (2008) Improvement of microcalcification cluster detection in mammography utilizing image enhancement techniques. Comput Biol Med 38: 1045–1055.
61. Kremers GJ, Goedhart J, vanMunster EB, Gadella TWJ (2006) Cyan and yellow super fluorescent proteins with improved brightness, protein folding, and FRET Förster radius. Biochemistry 45: 6570–6580.
62. Van Petegem F, Clark KA, Chatelain FC, Minor DL Jr (2004) Structure of a complex between a voltage-gated calcium channel β-subunit and an α-subunit domain. Nature 429: 671–675.
63. Kobrinsky E, Tiwari S, Maltsev VA, Harry JB, Lakatta E, et al. (2005) Differential role of the α_{1C} subunit tails in regulation of the $Ca_v1.2$ channel by membrane potential, β subunits, and Ca^{2+} ions. J Biol Chem 280: 12474–12485.
64. Chen Y-h, Li M-h, Zhang Y, He L-l, Yamada Y, et al. (2004) Structural basis of the α_1-β subunit interaction of voltage-gated Ca^{2+} channels. Nature 429: 675–680.
65. Opatowsky Y, Chen C-C, Campbell KP, Hirsch JA (2004) Structural analysis of the voltage-dependent calcium channel β subunit functional core and its complex with the α1 interaction domain. Neuron 42: 387–399.